International Journal of Minerals, Metallurgy and Materials
Volume 29, Number 9, September 2022, Page 1780
https://doi.org/10.1007/s12613-021-2322-2

Influence of multiple laser shock peening treatments on the microstructure and mechanical properties of Ti–6Al–4V alloy fabricated by electron beam melting

Liang Lan[1,2)✉], *Ruyi Xin*[1,2)], *Xinyuan Jin*[1)], *Shuang Gao*[1,2)], *and Bo He*[1,2)✉]

1) School of Material Engineering, Shanghai University of Engineering Science, Shanghai 201620, China
2) Research Center of High-temperature Alloy Precision Forming, Shanghai University of Engineering Science, Shanghai 201620, China
(Received: 5 February 2021; revised: 17 June 2021; accepted: 22 June 2021)

Abstract: Laser shock peening (LSP) is an attractive post-processing method to tailor surface microstructure and enhance mechanical performances of additive manufactured (AM) components. The effects of multiple LSP treatments on the microstructure and mechanical properties of Ti–6Al–4V part produced by electron beam melting (EBM), as a mature AM process, were studied in this work. Microstructure, surface topography, residual stress, and tensile performance of EBM-manufactured Ti–6Al–4V specimens were systematically analyzed subjected to different LSP treatments. The distribution of porosities in EBM sample was assessed via X-ray computed tomography. The results showed that EBM samples with two LSP treatments possessed a lower porosity value of 0.05% compared to the value of 0.08% for the untreated samples. The strength of EBM samples with two LSP treatments was remarkably raised by 12% as compared with the as-built samples. The grains of α phase were refined in near-surface layer, and a dramatic increase in the depth and magnitude of compressive residual stress (CRS) was achieved in EBM sample with multiple LSP treatments. The grain refinement of α phase and CRS with larger depth were responsible for the strength enhancement of EBM samples with two LSP treatments.

Keywords: additive manufacturing; laser shock peening; electron beam melting; residual stress; Ti–6Al–4V alloy; mechanical properties

1. Introduction

Ti–6Al–4V, as an α+β dual-phase titanium alloy, is broadly used in the aerospace, automotive, and medical sectors owing to its high strength, low density, good corrosion resistance, and biocompatibility [1–2]. However, Ti–6Al–4V components are difficult to fabricate with conventional processing methods because of their great chemical reactivity and low heat coefficient [3]. Additive manufacturing (AM) of metals, often known as metals 3D printing, refers to an advanced manufacturing process [4–6]. In particular, electron beam melting (EBM) is a mature powder-based AM method for the production of 3D near-net-shaped Ti–6Al–4V parts. As the energy provided via the electron beam is controllable, EBM has shown the possibility to produce near-full density metallic parts.

However, Ti–6Al–4V alloy fabricated by EBM process has a strong columnar grain structure and residual stress [7–8]. The columnar prior-β grains in as-prepared Ti–6Al–4V alloy exhibit the strong <001> orientation along the build direction (BD) [9]. And thus, the coarse prior-β grains and residual stresses further degrade the strength of EBM Ti–6Al–4V parts. Hence, it is crucial to change the microstructure and residual stress state in the near-surface layer via post-processing methods, such as laser shock peening (LSP) [10], shot peening (SP) [11], and surface mechanical attrition [12], for achieving AM metallic parts with acceptable mechanical performance.

LSP is an attractive surface modification method, wherein a high pressure shockwave is induced via the interaction between materials and high-energy pulsed laser [13–14]. Compared with conventional SP, LSP process is capable to generate a higher compressive residual stress (CRS) with a larger depth. Besides, enhancements in fatigue lifetime, tensile strength, and microhardness have extensively been investigated via LSP treatment [15–17]. Recently, a few studies have paid more attention to the effect of LSP on AM metallic parts [18–19]. Kalentics *et al*. [20] described that LSP elevates the stored strain energy in SLM-fabricated 316L stainless steel part and enhances the recrystallization kinetics during heat treatment. Sun *et al*. [21] showed that LSP can refine the microstructure of wire-arc AM 2319 aluminum part and increase yield strength of the part. Lu *et al*. [22] demonstrated that LSP tailors the surface microstructure and mechanical performances of selective laser melted (SLM) Ti–6Al–4V sample and produces CRS with maximum of ~396 MPa and a depth of 900 μm. In our previous work, LSP has been served as a post-treatment process for EBM-built Ti–6Al–4V alloy to refine microstructure and enhance the mechanical properties [23]. However, the interac-

✉ Corresponding authors: Liang Lan Email: lanliang@sues.edu.cn; Bo He Email: hebo@sues.edu.cn
© University of Science and Technology Beijing 2022

tion between shockwaves and the microstructural changes generated in EBM sample with multiple LSP treatments is still pending. In fact, multiple LSP treatments may be the more effective method to significantly increase the CRS in depth direction. Lu *et al*. [24] showed that the improvement of residual stress is associated with the generation of the dislocation and the micro-structural deformation near the surface during multiple LSP treatments. Therefore, the effects of multiple LSP on the microstructure and mechanical performances of as-fabricated Ti–6Al–4V components deserve further investigation.

The goal of this work is to explore mechanical property and microstructure strengthening mechanism of EBM-built Ti–6Al–4V alloy with multiple LSP treatments. Microstructure evolution, residual stresses, surface topographies, porosities, and the tensile strength of EBM Ti–6Al–4V samples after being subjected to multiple LSP treatments were examined. The enhancement mechanism in strength of EBM sample with multiple LSP was discussed.

2. Experimental

EBM manufacturing was conducted on an Arcam A2X machine (Arcam AB, Sweden). Gas atomized Ti–6Al–4V ELI powder supplied by Arcam AB was used as raw material. The particle size of the powder is ranging from 45 to 105 μm. Table 1 shows chemical composition of the Ti–6Al–4V powder. The process was conducted under a vacuum of 10^{-1} Pa, and the preheat temperature was controlled at 1023 K. The EBM manufacturing parameters of the build included layer thickness of 0.05 mm, scanning speed of 4530 mm/s, and beam intensity of 15 mA. The EBM machine adopted a strategy of line scanning using a 90° change between layers for better density and mechanical performance. After the samples were fabricated via EBM process, they were subjected to multiple LSP treatments.

Table 1. Chemical composition of received Ti–6Al–4V powder

wt%

Al	V	C	Fe	O	N	H	Ti
6.0	4.0	0.03	0.1	0.1	0.01	<0.003	Balance

LSP treatments were conducted using a Q-switched Nd:YAG laser system operated at a wavelength of 1064 nm. The LSP parameters were as follows: pulse duration of 12 ns; spot size diameter of 2.5 mm; overlapping rate of 25%. The samples were protected by the absorbing and water spraying layers before irradiation. The LSP process for EBM specimen was schematically described in Fig. 1. The laser power density was 11.89 GW/cm^2. Detail experiments were described in our previous study [23].

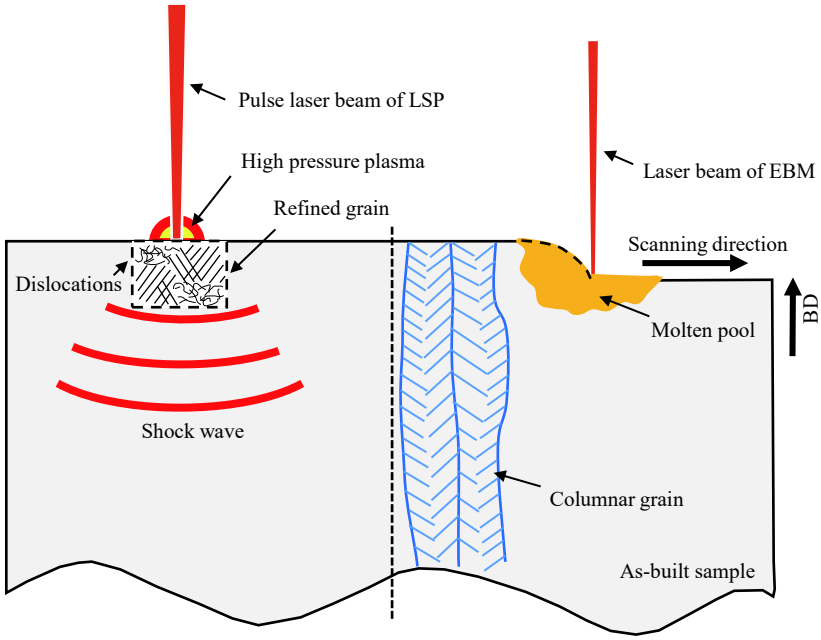

Fig. 1. Schematic of EBM combined with LSP.

The samples were ground on silicon carbide papers with various roughness grades (up to 2000), polished using diamond suspensions, and etched by a solution of 50 mL distilled water, 25 mL nitric acid, and 5 mL hydrofluoric acid. Optical microscope (OM), electron back-scatter diffraction (EBSD), and X-ray diffraction (XRD) were used to characterize the microstructure and phase composition of the specimens. Surface topographies of the specimens with multiple LSP treatments were analyzed via white light interferometer. A Proto LXRD (Proto, Canada) instrument was conducted to measure the residual stresses of EBM samples using conventional XRD with the $\sin^2\psi$ method. Lattice strain measurement was conducted at the {213}-planes of the hexagonal a-phase. The X-ray tube voltage and current were 30 kV and 25 mA, respectively. To obtain the distribution of 3D porosity, EBM specimens were examined via the X-ray computed

tomography (XCT, North Star Imaging, USA) with multiple LSP treatments. Specimens with dimensions of 8 mm × 8 mm × 2 mm were placed on the rotating stage in front of the X-ray source with a minimum focal spot size of 4.9 μm. The tomography was performed at a current of 35 μA and an acceleration voltage of 140 kV. The specimens were rotated 360° around and a series of 2D images were captured, to realize the 3D reconstruction.

In addition, tensile tests of EBM specimens with multiple LSP treatments were conducted as per GBT228-2002 standard using a strain rate of 0.5 mm/min. The specimens were tested normal to the BD. LSP treatments were carried out on two sides covering the gauge length region. The specimens gauge section was 4 mm × 2 mm. Three specimens were performed for each condition to achieve reliable results. The ultimate tensile strength (UTS), yield strength (YS), and elongation (El) of EBM specimens were examined, and the fracture morphologies were analyzed using the scanning electron microscopy (SEM).

3. Results

3.1. Microstructure and phase analysis

OM observations were conducted for investigating the microstructural features formed during EBM. A columnar crystal can be faintly observed in the cross-section of EBM-built Ti–6Al–4V sample shown in Fig. 2(a), which are oriented parallel to BD. Every columnar crystal has β+α lamella structure, with no visible pores or cracks in the as-built specimen. Compared to the SLM process, the cooling rate is low in the EBM process, and thus, it is universally acknowledged that the microstructure of as-prepared EBM Ti–6Al–4V samples consists of the stable β and α phases, rather than metastable α′ phase [8]. Fig. 2(b) presents the XRD pattern of EBM-built specimen before and after LSP treatments. There are mainly composed of β and α phases, and none of the new phase is observed subjected to two LSP treatments. In addition, the diffraction peaks are broadened and shift to lower angles after two LSP treatments. According to the Bragg equation, the lattice parameters of α-Ti and β-Ti phases were obtained without LSP and after two LSP treatments, as listed in Table 2. The broadening of the peaks after LSP indicates dislocation density increasing and grain refinement, while the shift of the peaks to smaller angles suggests the existence of anisotropic residual stress and an increase in lattice parameters.

Fig. 3 presents the cross-sectional EBSD maps and grain sizes of EBM Ti–6Al–4V samples subjected to different LSP treatments. The EBSD orientation image maps exhibit the grain features of EBM samples without and two LSP treatments in Fig. 3(a) and (b). The distinct difference in gain size and crystal orientation can be found. The prior-β columnar grains paralleling to BD are observed in Fig. 3(a), including α colonies or basket-weave microstructure. The color codes of EBM samples subjected to LSP treatments indicate orientations of the grains at random crystallographic directions, as shown in Fig. 3(b). In addition, blurry boundaries between prior-β columnar grains are found in LSP-treated samples (Fig. 3(b)). The prior columnar grains in near-surface zone are markedly refined with two LSP treatments. It is observed that the thickness of α lath in EBM sample decreases after LSP treatments compared Fig. 3(c) with Fig. 3(d). The grain sizes of α phase are refined which could be ascribed to the severe plastic deformation with LSP treatments [13]. Grain refinement is a conducive approach for improving the mechanical performances of metallic materials, which can enhance the strength of EBM-built parts.

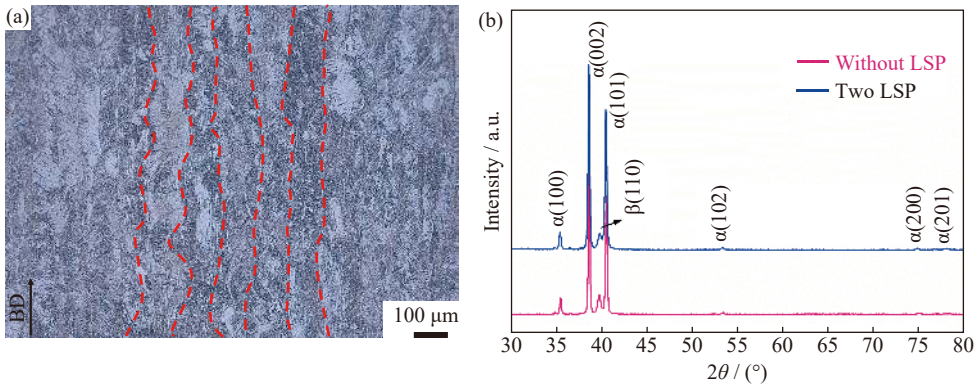

Fig. 2. (a) OM image and (b) XRD pattern of EBM Ti–6Al–4V sample with different LSP treatments.

Table 2. Lattice parameters of the α and β phases with different LSP treatments

Sample	α-Ti		β-Ti
	a / nm	c / nm	a_β / nm
Without LSP	0.29273	0.46710	0.32059
2 LSP treatments	0.29337	0.46793	0.32149

3.2. Porosity

The 3D visualization of EBM Ti–6Al–4V specimens without LSP and after two LSP treatments are presented in Fig. 4. Pore sizes were measured as the equivalent diameter for a spherical representation of pores. The color distribution represents the equivalent diameter of the pores. The minimum diameter of EBM samples was determined as 19 μm. At the same time, the porosities fraction of EBM samples was calculated according to the volume ratio between the all detected pores and the samples. After two LSP treatments, the average size of the pores was decreased from the untreated sample diameter of 33.9 to 30.5 μm. The summary of poros-

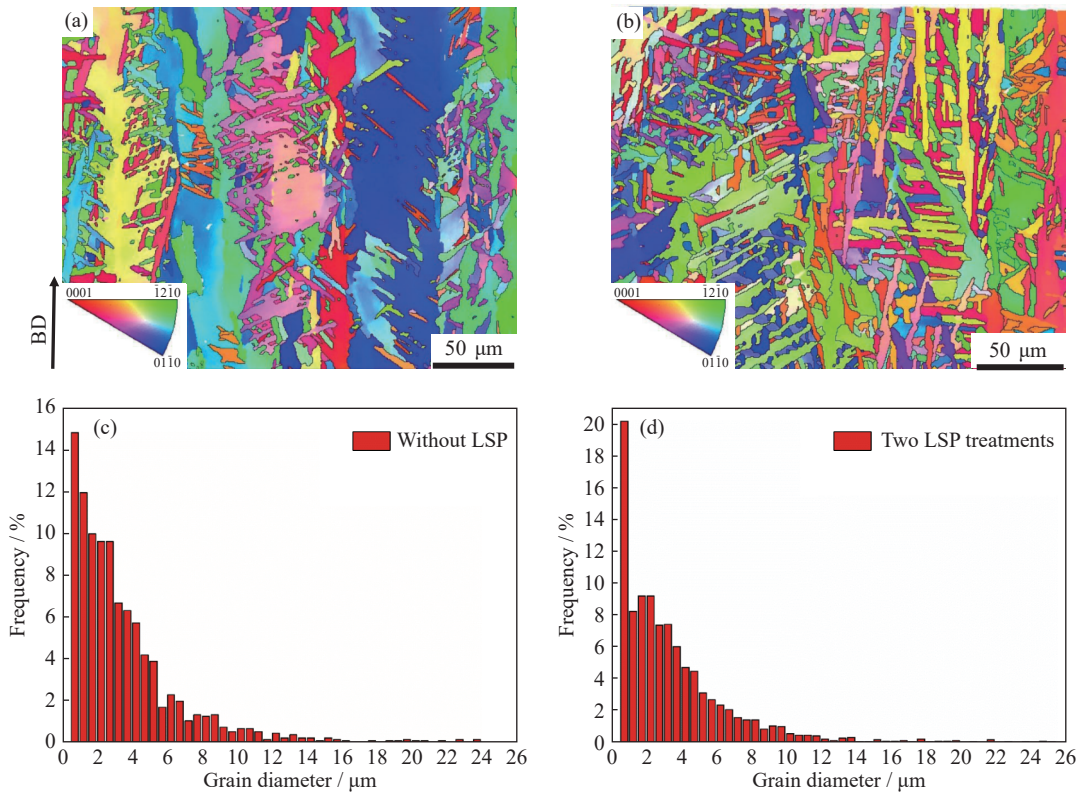

Fig. 3. EBSD maps (a, b) and grain size (c, d) of the cross-section for EBM Ti–6Al–4V samples subjected to different LSP treatments: (a, c) without LSP and (b, d) after two LSP treatments.

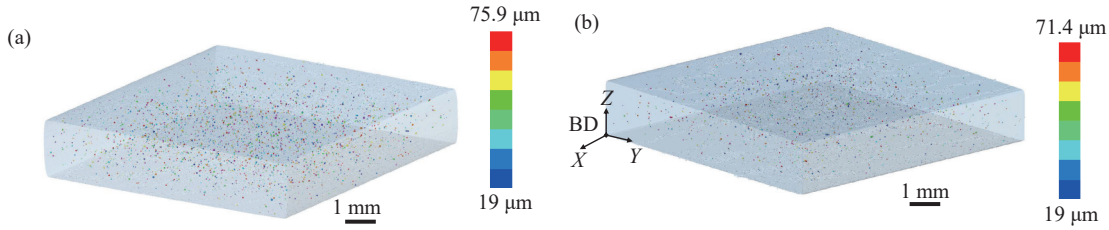

Fig. 4. 3D reconstruction of porosity of EBM-fabricated Ti–6Al–4V samples subjected to different LSP treatments: (a) without LSP and (b) after two LSP.

ity analysis for EBM samples with different LSP treatments is illustrated in Table 3. From Table 3, the EBM sample without LSP was achieved with a porosity value of 0.08%. After two LSP treatments, EBM sample possessed a slight lower porosity value of 0.05% compared to the untreated sample.

3.3. Surface morphology

Fig. 5 shows 3D surface topographies of EBM Ti–6Al–4V specimens without LSP and after two LSP treatments. It can be observed that obvious micro dimples appear on the surface of EBM specimens with LSP treatments in Fig. 5(b), compared with the untreated sample in Fig. 5(a). It is attributed to the plastic flow of EBM samples produced via high pressure shockwaves during LSP. The vertical fluctuation of micro dimples induced via LSP impacts relates to the microhardness and strength of the EBM samples to some extent. Moreover, it is observed that the profile of the dimples in LSP-treated sample is analogous to the spherical cap whose inside-wall is inclined rather than vertical. Li *et al.* [25] described that LSP treatment produces 3D topographies of micro dimples on the surface of stainless steel, aluminum alloy, and copper, indicating that severe plastic deformation is generated during LSP.

Table 3. XCT porosity measurements of the samples with different LSP treatments

Sample	Equivalent diameter / mm		Defect volume / mm^3	Porosity / %
	Min	Max		
Without LSP	0.0190	0.0759	0.0643	0.08
Two LSP	0.0190	0.0714	0.0490	0.05

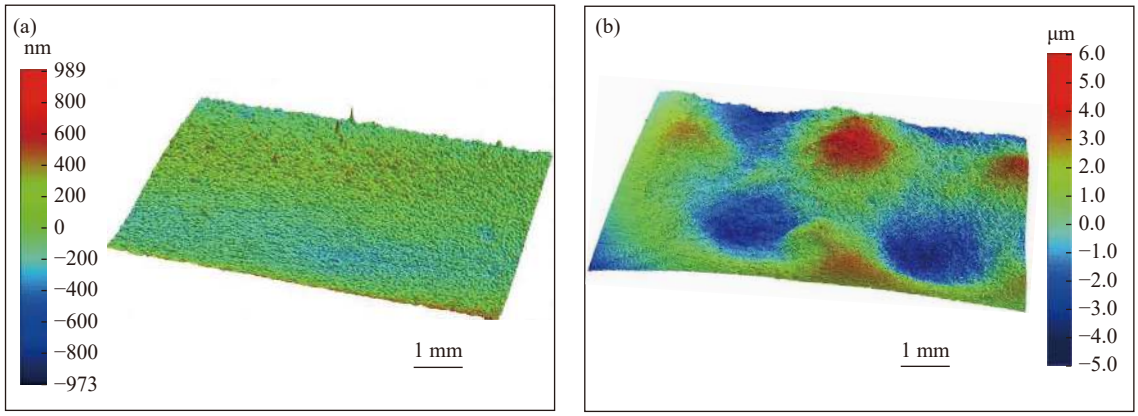

Fig. 5. 3D surface topographies of EBM-fabricated Ti–6Al–4V samples with different LSP treatments: (a) without LSP and (b) after two LSP.

3.4. Residual stress

Fig. 6 illustrates the residual stresses profiles of EBM Ti–6Al–4V specimens subjected to different LSP impacts with depth. It is observed that the residual stress of approximate ±50 MPa is produced at the surface of EBM-fabricated sample without LSP, which is lower than the residual stress of SLM-built parts [26–27]. LSP modifies the surface stress state and the maximum CRS of −419 MPa is formed on the surface in EBM sample with two LSP treatments. The CRS reduces and converts into tensile residual stress with elevating depth away from the surface. Notably, the plastically affected depth of the sample is up to 700 μm after being subjected to two LSP treatments, which is larger than the hardening depth in as-prepared Ti–6Al–4V specimen after single LSP treatment [23], as shown in Fig 6.

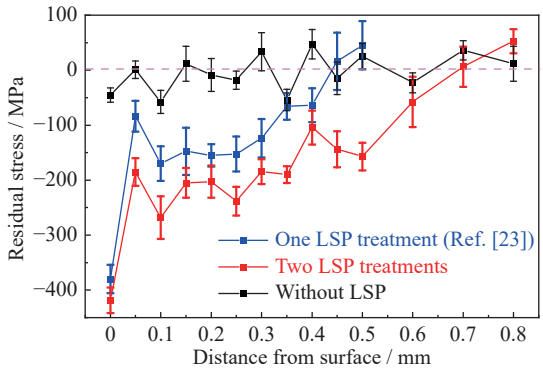

Fig. 6. In-depth residual stress of EBM samples with different LSP treatments.

3.5. Mechanical properties and fractographies

The room temperature tensile properties of EBM Ti–6Al–4V samples with different LSP treatments were investigated. Fig. 7 illustrates the typical engineering stress–strain plots of EBM samples subjected to multiple LSP treatments. Notably, the strength of EBM specimens with multiple LSP treatments is superior to those of the untreated specimens. The tensile load is conducted orthogonal to the BD. Table 4 displays UTS, YS, and El of the specimens with different LSP treatments. It has been shown that the YS and UTS of the specimens are significantly enhanced and the El slightly reduces subjected to two LSP treatments. The UTS of the EBM samples with two LSP treatments raises from 916 to 1026 MPa, that is, an increase of 12% in UTS. Comparing with the EBM-built Ti–6Al–4V samples subjected to single LSP treatments [23], the EBM samples with two LSP treatments increases by 7% and 6% in UTS and YS, respectively. In present work, the grain refinement and affected layers of CRS with larger depth are achieved in EBM samples after being subjected to two LSP treatments, which can be the main factors for strength enhancement.

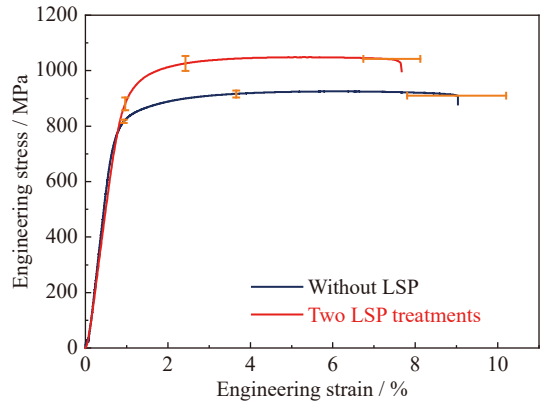

Fig. 7. Engineering stress–strain curves of EBM Ti–6Al–4V samples with different LSP treatments.

Table 4. Mechanical properties of EBM specimens subjected to different LSP treatments

Sample	UTS / MPa	YS / MPa	El / %
Without LSP	916 ± 12.73	817 ± 5.66	9.30 ± 1.56
2 LSP treatments	1026 ± 27.18	879.67 ± 22.98	7.43 ± 0.69

Fig. 8 displays SEM fracture morphologies of EBM specimens without LSP and after two LSP treatments. Fig. 8(a) and (b) show the fracture surface of EBM specimens without LSP, while Fig. 8(c) and (d) are EBM specimens with two LSP treatments. It is featured via microcrack, micro-voids, and inhomogeneous dimples, suggesting that EBM specimen without LSP are ductile fracture. Micro-voids in the surface of the untreated EBM specimen are possibly the source

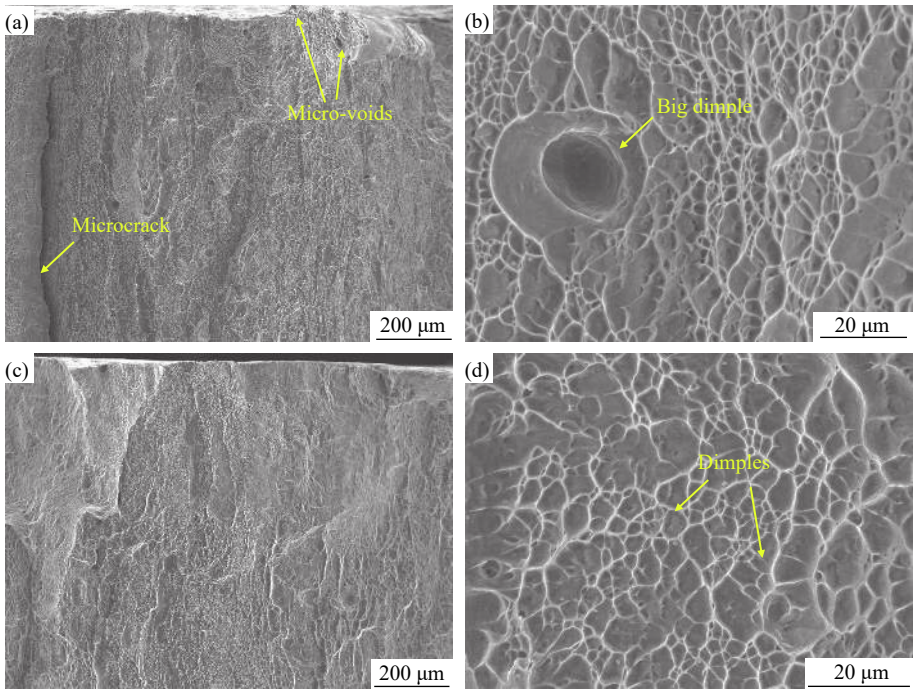

Fig. 8. Fracture morphologies of EBM samples subjected to different LSP treatments: (a,b) without LSP and (c, d) after two LSP treatments.

of the fracture. For the EBM specimen with two LSP treatments, deeper dimples with relatively homogeneous sizes are found, and no obvious microcracks are observed. Fractographic analysis shows that both specimens subjected to different LSP treatments exhibit ductile fracture.

4. Discussion

4.1. Influence of LSP on porosity

It is well known that the pressure induced via surface treatment process may result in the closing of porosities in samples. Sun *et al*. [28] showed that LSP is a helpful approach for decreasing the pores size of laser-welded aluminum alloy joints. Dekhtyar *et al*. [29] reported that ultrasonic impact treatment can heal micro-pores of powder metallurgy Ti–6Al–4V samples and enhance the fatigue life of the samples. Kalentics *et al*. [30] described that the density of SLM-built, LSP, and 3D LSP 316 L stainless steel specimens is 99.82 %, 99.87 %, and 99.84 %, respectively, indicating LSP treatment can decrease pores size and aspect ratio, and enhance fatigue properties of SLM samples. According to our XCT results, LSP-treated EBM samples possessed a lower porosity value compared to the untreated samples, which indicates that LSP treatments contribute closing pores in EBM sample. There are usually two types of pores in AM parts: gas pores and lack-of-fusion pores [1,31]. Gas pores are formed due to the gas entrapment such that the gas trapped in the molten pool does not escape in time and is hence stuck in the solidified bead. Lack-of-fusion pores are mainly produced because of deviation from optimal melting conditions, which results in inadequate melting and weak bonding between layers. As LSP is a cold-working process, the decrease of porosity can only be resulted from the plastic deformation under high-dynamic shock loading. Since the weakness of bearing capacity around a pore, more severe plastic deformation can be generated around a pore to decrease the pore size and quantity after LSP treatment. Besides, the pores because of the insufficient deformation were present in untreated EBM specimen, which probably become the fracture source during a tensile test, as shown in Fig. 8(a). Meanwhile, the decrease of pores after being subjected to LSP can avoid the stress concentration and crack propagation during the test and enhance tensile properties of the samples. Thus, the closing of porosities after being subjected to LSP treatments is favorable for tensile and fatigue properties of AM parts.

4.2. Influence of LSP on stress state

The residual stresses profiles of EBM specimens with depth in Fig. 6 indicated that two LSP treatments give raise to apparent improvement in compressive stress together with a depth of 700 μm. It is well known that laser shockwave spreading into the sample follows a Gauss distributed pressure induced at the surface during LSP. While the pressure exceeds metal's Hugoniot elastic limit [32], it will induce residual stress. Owing to the shallow depth at which the X-rays penetrate the surface, the measured stress is approximately a plane stress, that is, stress in the direction perpendicular to the surface is zero. With the action of pulse laser, the elongation deformation in the plane parallel to the surface occurs, but the elongation of the surface layer is restrained via the undeformed layer below, which leads to beneficial CRS. In order to balance the CRS, the tensile stress produces in the undeformed zone. As the laser pulse wave transmits into the sample, the pressure amplitude reduces with depth, when the deformation of the sample continuously proceeds until it is

lower than the dynamic YS. Therefore, the CRS changes with the affected depth.

Moreover, it is notable via comparing residual stress distribution in LSP-treated EBM sample with an as-built sample that the greater the CRS is, the greater the balance tensile residual stress is. In EBM sample a small tensile stress in surface layer balances a small CRS, and such small stress (±50 MPa) is ascribed to stress relief arisen from the preheating temperature of 1023 K in EBM. For LSP-treated sample, a great CRS of around −419 MPa on the surface was induced, and therefore a large tensile residual stress for the balance would be generated in undeformed layer, the depth of which was much higher than 700 μm demonstrated in Fig. 6. The introduction of CRS layer with larger depth exhibits a prominent influence on the fatigue performance of AM parts [30,33].

4.3. Strengthening mechanism induced via LSP

Grain refinement is commonly beneficial to the strength of metals or alloys on the basis of the Hall-Petch relation [34]. It is ascribed to the effect of grain boundaries that block dislocations sliding and elevate the resistance for dislocations traversing grain boundaries [35]. From Fig. 3(b), the refined α lamellar microstructure was remarkably observed in EBM-built samples after two LSP treatments. Tensile strength enhancement in EBM specimens with LSP treatments is attributed to grain refinement of α phase. Meanwhile, grain refinement results in the decrease in ductility for EBM specimens. Additionally, pores have an important influence on the tensile strength of EBM samples. The closing of porosities in the subsurface region of the sample is beneficial to tensile properties of EBM parts. It is universally acknowledged that LSP is capable of generating more than 100 MPa CRS at the surface in the sample. The residual stresses distribution of EBM samples with depth indicated that LSP treatments induce the maximum compressive stress of −419 MPa accompanying with a depth of 700 μm. The high CRS arisen from two LSP treatments is conductive to closing pores and decreasing their sizes. Meantime, the CRS reversed part of tensile residual stress during tensile tests. Therefore, the strengthening mechanism for EBM samples after being subjected to two LSP treatments is attributed to the effects of grain refinement of α phase and compressive stress with larger depth.

5. Conclusions

The influences of multiple LSP treatments on the microstructure and mechanical properties of Ti–6Al–4V samples produced by EBM process were studied. Microstructure evolution, residual stress, surface topography, pore profile, and tensile property of as-built samples were characterized subjected to different LSP treatments. The following conclusions from this work are summarized.

(1) The residual stress profiles illustrated that two LSP treatments produced maximum CRS of around −419 MPa at the surface of EBM samples with a depth of 700 μm, which was larger than the depth in as-prepared specimen after single LSP impact. EBSD results showed that the grains of α phase were refined in near-surface layer in EBM sample with two LSP treatments.

(2) After being subjected to two LSP treatments, EBM samples possessed a lower porosity value of 0.05% compared to the porosity value of 0.08% for the untreated samples based on the XCT results.

(3) Compared with the EBM Ti–6Al–4V samples, tensile strength of EBM samples after two LSP treatments was raised via 12% from 916 to 1026 MPa. The tensile strength of EBM specimens with two LSP treatments was dramatically improved, which was primarily attributed to grain refinement of α phase and CRS with larger depth.

These results show the potential for multiple LSP treatments to be applied to improve fatigue performance of AM parts.

Acknowledgements

This work was financially supported by the Shanghai Science and Technology Committee Innovation Grant (Nos. 17JC1400600 and 17JC1400603) and the Distinguished Professor Program of Shanghai University of Engineering Science. The authors thank Zhishui Yu for preparing EBM samples and Y. Morris Wang of Lawrence Livermore National Laboratory for helpful discussions.

Conflict of Interest

The authors declare no potential conflict of interest.

References

[1] S.Y. Liu and Y.C. Shin, Additive manufacturing of Ti6Al4V alloy: A review, *Mater. Des.*, 164(2019), art. No. 107552.

[2] J.M. Manero, F.J. Gil, and J.A. Planell, Deformation mechanisms of Ti–6Al–4V alloy with a martensitic microstructure subjected to oligocyclic fatigue, *Acta Mater.*, 48(2000), No. 13, p. 3353.

[3] T. Voisin, N.P. Calta, S.A. Khairallah, J.B. Forien, L. Balogh, R.W. Cunningham, A.D. Rollett, and Y.M. Wang, Defects-dictated tensile properties of selective laser melted Ti–6Al–4V, *Mater. Des.*, 158(2018), p. 113.

[4] Y.M. Wang, T. Voisin, J.T. McKeown, J. Ye, N.P. Calta, Z. Li, Z. Zeng, Y. Zhang, W. Chen, T.T. Roehling, R.T. Ott, M.K. Santala, P.J. Depond, M.J. Matthews, A.V. Hamza, and T. Zhu, Additively manufactured hierarchical stainless steels with high strength and ductility, *Nat. Mater.*, 17(2018), No. 1, p. 63.

[5] C.Y. Chen, Y.C. Xie, X.C. Yan, S. Yin, H. Fukanuma, R.Z. Huang, R.X. Zhao, J. Wang, Z.M. Ren, M. Liu, and H.L. Liao, Effect of hot isostatic pressing (HIP) on microstructure and mechanical properties of Ti6Al4V alloy fabricated by cold spray additive manufacturing, *Addit. Manuf.*, 27(2019), p. 595.

[6] D. Zhang, D. Qiu, M.A. Gibson, Y. Zheng, H.L. Fraser, D.H. StJohn, and M.A. Easton, Additive manufacturing of ultrafine-grained high-strength titanium alloys, *Nature*, 576(2019), No. 7785, p. 91.

[7] A.T. Silvestri, S. Foglia, R. Borrelli, S. Franchitti, C. Pirozzi, and A. Astarita, Electron beam melting of Ti6Al4V: Role of the

process parameters under the same energy density, *J. Manuf. Processes*, 60(2020), p. 162.
[8] X.Q. Wang and K. Chou, EBSD study of beam speed effects on Ti–6Al–4V alloy by powder bed electron beam additive manufacturing, *J. Alloys Compd.*, 748(2018), p. 236.
[9] A.A. Antonysamy, J. Meyer, and P.B. Prangnell, Effect of build geometry on the β-grain structure and texture in additive manufacture of Ti6Al4V by selective electron beam melting, *Mater. Charact.*, 84(2013), p. 153.
[10] S. Kalainathan and S. Prabhakaran, Recent development and future perspectives of low energy laser shock peening, *Opt. Laser Technol.*, 81(2016), p. 137.
[11] S.J. Lainé, K.M. Knowles, P.J. Doorbar, R.D. Cutts, and D. Rugg, Microstructural characterisation of metallic shot peened and laser shock peened Ti–6Al–4V, *Acta Mater.*, 123(2017), p. 350.
[12] X.C. Yan, S. Yin, C.Y. Chen, R. Jenkins, R. Lupoi, R. Bolot, W.Y. Ma, M. Kuang, H.L. Liao, J. Lu, and M. Liu, Fatigue strength improvement of selective laser melted Ti6Al4V using ultrasonic surface mechanical attrition, *Mater. Res. Lett.*, 7(2019), No. 8, p. 327.
[13] C.S. Montross, T. Wei, L. Ye, G. Clark, and Y.W. Mai, Laser shock processing and its effects on microstructure and properties of metal alloys: A review, *Int. J. Fatigue*, 24(2002), No. 10, p. 1021.
[14] P. Peyre, C. Carboni, P. Forget, G. Beranger, C. Lemaitre, and D. Stuart, Influence of thermal and mechanical surface modifications induced by laser shock processing on the initiation of corrosion pits in 316L stainless steel, *J. Mater. Sci.*, 42(2007), No. 16, p. 6866.
[15] K.Y. Luo, J.Z. Lu, Q.W. Wang, M. Luo, H. Qi, and J.Z. Zhou, Residual stress distribution of Ti–6Al–4V alloy under different ns-LSP processing parameters, *Appl. Surf. Sci.*, 285(2013), p. 607.
[16] W.J. Jia, Q. Hong, H.Z. Zhao, L. Li, and D. Han, Effect of laser shock peening on the mechanical properties of a near-α titanium alloy, *Mater. Sci. Eng. A*, 606(2014), p. 354.
[17] J. Wang, Y.L. Lu, D.S. Zhou, L.Y. Sun, L. Xie, and J.T. Wang, Mechanical properties and microstructural response of 2A14 aluminum alloy subjected to multiple laser shock peening impacts, *Vacuum*, 165(2019), p. 193.
[18] L. Hackel, J.R. Rankin, A. Rubenchik, W.E. King, and M. Matthews, Laser peening: A tool for additive manufacturing post-processing, *Addit. Manuf.*, 24(2018), p. 67.
[19] W. Guo, R.J. Sun, B.W. Song, Y. Zhu, F. Li, Z.G. Che, B. Li, C. Guo, L. Liu, and P. Peng, Laser shock peening of laser additive manufactured Ti6Al4V titanium alloy, *Surf. Coat. Technol.*, 349(2018), p. 503.
[20] N. Kalentics, K. Huang, M. Ortega Varela de Seijas, A. Burn, V. Romano, and R.E. Logé, Laser shock peening: A promising tool for tailoring metallic microstructures in selective laser melting, *J. Mater. Process. Technol.*, 266(2019), p. 612.
[21] R.J. Sun, L.H. Li, Y. Zhu, W. Guo, P. Peng, B.Q. Cong, J.F. Sun, Z.G. Che, B. Li, C. Guo, and L. Liu, Microstructure, residual stress and tensile properties control of wire-arc additive manufactured 2319 aluminum alloy with laser shock peening, *J. Alloys Compd.*, 747(2018), p. 255.
[22] J.Z. Lu, H.F. Lu, X. Xu, J.H. Yao, J. Cai, and K.Y. Luo, High-performance integrated additive manufacturing with laser shock peening-induced microstructural evolution and improvement in mechanical properties of Ti6Al4V alloy components, *Int. J. Mach. Tools Manuf.*, 148(2020), art. No. 103475.
[23] L. Lan, X.Y. Jin, S. Gao, B. He, and Y.H. Rong, Microstructural evolution and stress state related to mechanical properties of electron beam melted Ti–6Al–4V alloy modified by laser shock peening, *J. Mater. Sci. Technol.*, 50(2020), p. 153.
[24] J.Z. Lu, K.Y. Luo, Y.K. Zhang, C.Y. Cui, G.F. Sun, J.Z. Zhou, L. Zhang, J. You, K.M. Chen, and J.W. Zhong, Grain refinement of LY2 aluminum alloy induced by ultra-high plastic strain during multiple laser shock processing impacts, *Acta Mater.*, 58(2010), No. 11, p. 3984.
[25] K.M. Li, Y.X. Hu, and Z.Q. Yao, Experimental study of micro dimple fabrication based on laser shock processing, *Opt. Laser Technol.*, 48(2013), p. 216.
[26] N. Kalentics, E. Boillat, P. Peyre, C. Gorny, C. Kenel, C. Leinenbach, J. Jhabvala, and R.E. Logé, 3D Laser Shock Peening − A new method for the 3D control of residual stresses in Selective Laser Melting, *Mater. Des.*, 130(2017), p. 350.
[27] L. Lan, R.Y. Xin, X.Y. Jin, S. Gao, B. He, Y.H. Rong, and N. Min, Effects of laser shock peening on microstructure and properties of Ti–6Al–4V titanium alloy fabricated via selective laser melting, *Materials*, 13(2020), No. 15, art. No. 3261.
[28] G. Sun, X. Fang, Z. Tong, Z. Ni, and Y. Lu, Effect of laser shock peening on aluminium alloy laser-welds, *Surf. Eng.*, 32(2016), No. 12, p. 943.
[29] A.I. Dekhtyar, B.N. Mordyuk, D.G. Savvakin, V.I. Bondarchuk, I.V. Moiseeva, and N.I. Khripta, Enhanced fatigue behavior of powder metallurgy Ti–6Al–4V alloy by applying ultrasonic impact treatment, *Mater. Sci. Eng. A*, 641(2015), p. 348.
[30] N. Kalentics, M.O.V. de Seijas, S. Griffiths, C. Leinenbach, and R.E. Logé, 3D laser shock peening - A new method for improving fatigue properties of selective laser melted parts, *Addit. Manuf.*, 33(2020), art. No. 101112.
[31] Y.W. Luo, M.Y. Wang, J.G. Tu, Y. Jiang, and S.G. Jiao, Reduction of residual stress in porous Ti6Al4V by *in situ* double scanning during laser additive manufacturing, *Int. J. Miner. Metall. Mater.*, 28(2021), No. 11, pp. 1844-1853.
[32] J.N. Johnson and R.W. Rohde, Dynamic deformation twinning in shock-loaded iron, *J. Appl. Phys.*, 42(1971), No. 11, p. 4171.
[33] X.Y. Jin, L. Lan, S. Gao, B. He, and Y.H. Rong, Effects of laser shock peening on microstructure and fatigue behavior of Ti–6Al–4V alloy fabricated via electron beam melting, *Mater. Sci. Eng. A*, 780(2020), art. No. 139199.
[34] F. Yin, G.J. Cheng, R. Xu, K.J. Zhao, Q. Li, J. Jian, S. Hu, S.H. Sun, L.C. An, and Q.Y. Han, Ultrastrong nanocrystalline stainless steel and its Hall-Petch relationship in the nanoscale, *Scripta Mater.*, 155(2018), p. 26.
[35] A. Di Schino and J.M. Kenny, Grain refinement strengthening of a micro-crystalline high nitrogen austenitic stainless steel, *Mater. Lett.*, 57(2003), No. 12, p. 1830.